only for that short period of time the powder could be in contact with air. The Kissinger method was used for calculation of the apparent energy of dehydriding according to the procedure described in detail in Ref. [1].

Finally, it must be pointed out that all the tests described in the following sections were carried out within a couple of days from the completion of ball milling of powders in order to avoid any long-term storage degradation effects.[1]

3. RESULTS AND DISCUSSION

Figure 2 shows a comparison of the XRD patterns for as received $NaAlH_4$, ball milled $NaAlH_4$ and the ball milled $NaAlH_4 + 5$ wt% n-Ni nanocomposite. It is clearly seen that the principal phase, before and after ball milling, is $NaAlH_4$ and a minority phase in the doped nanocomposite is obviously nanometric Ni (n-Ni). High energy ball milling does not induce any phase transformation which means that neither decomposition of $NaAlH_4$ nor reaction of n-Ni with the matrix occurred during milling. The diffraction peaks of $NaAlH_4$ in the ball milled powders are broadened which is mainly related to the refinement of grain/crystallite size within the individual particles. We did not estimate the exact grain size of ball milled $NaAlH_4$ in this work. However, for a similar alanate hydride, $LiAlH_4$, ball milled for the same time duration of 15 min, we estimated the average grain/crystallite size from the peak broadening of Bragg peaks in XRD patterns, as being on the order of 80 nm.[16] Since crystalline structure of both $NaAlH_4$ and $LiAlH_4$ is quite similar[22] one can reasonably assume that the grain/crystallite size of $NaAlH_4$ ball milled for 15 min in this work could be roughly on the order of 80 nm which is close to the upper limit for nanocrystallinity. In general, we have found on a number of occasions from XRD measurements that the grain/crystallite size of as received alanates ($NaAlH_4$ and $LiAlH_4$) is larger than 100 nm although it is hard to assess the exact size since the method of estimating the grain/crystallite size from the broadening of XRD becomes very inaccurate for sizes larger than 100 nm.[23] Therefore, it seems that high energy ball milling of $NaAlH_4$ and $LiAlH_4$ is not so effective in reducing their initial grain size much below 100 nm range.

The XRD patterns in Figure 2 also show some presence of very small impurity peaks (as mentioned earlier, we intentionally used unpurified hydride since the purification would substantially increase its cost for any perceived commercial applications). We made an effort to identify those impurity peaks but most compounds which we tried to fit such as various sodium hydroxides, sodium oxides, aluminum oxide, aluminum hydroxide, sodium-aluminum oxide, sodium hydride and sodium chloride did not fit to the observed peaks. The only chemical compounds whose XRD patterns fit very well are $Al_{29}(OH)_{78}Cl_9$ (JCPDS 13-0320) and $AlCl_3 \cdot 6H_2O$ (JCPDS 08-0453 and 44-1473). In conclusion, it seems that the impurities existing in this technical purity $NaAlH_4$ may be some complex aluminum chlorides which point towards their origin in the production process of the powder.

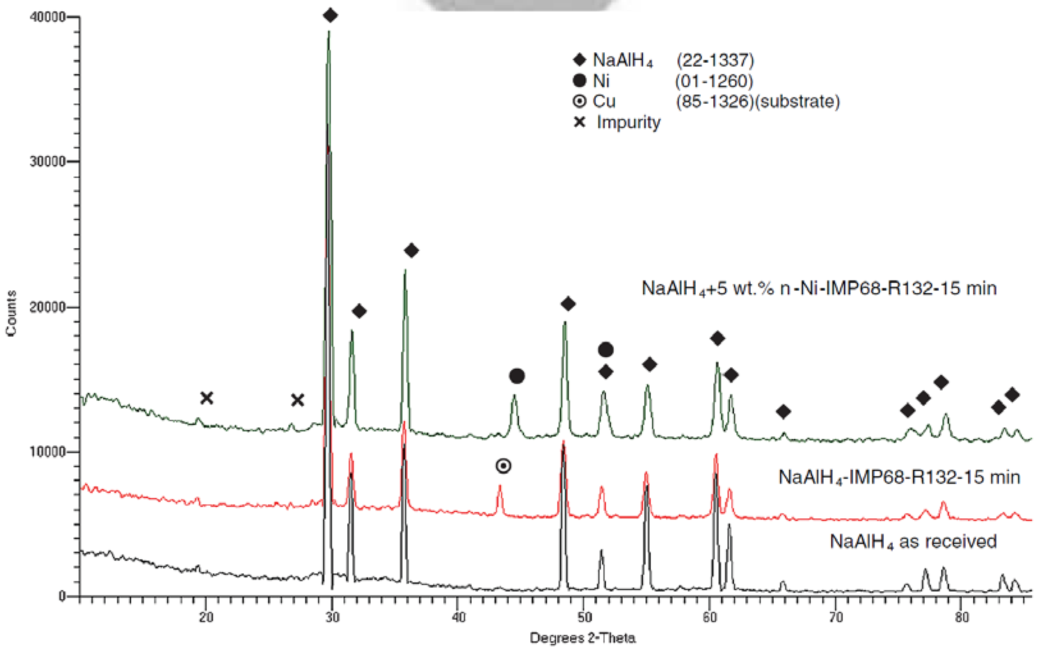

Fig. 2. A comparison of the XRD patterns for as received $NaAlH_4$, ball milled $NaAlH_4$ and the ball milled $NaAlH_4 + 5$ wt% n-Ni nanocomposite. JCPDS file numbers for identification are shown.

Figures 3(a–c) show the DSC curves for as received $NAlH_4$, ball milled $NaAlH_4$ and ball milled $NaAlH_4$ + 5 wt% n-Ni, respectively. In Figure 3(a) each peak is assigned to the specific reaction as discussed earlier in the text. The first peak is exothermic and its origin is not completely clear. This first exotherm for as received $NaAlH_4$ at 174.3 °C in Figure 3(a), 167.6 °C for milled $NaAlH_4$ in Figure 3(b) and 165.7 °C for milled $NaAlH_4$ + 5 wt% n-Ni in Figure 3(c), was attributed by Block and Gray,[24] who investigated the thermal decomposition of $LiAlH_4$, to the reaction of the surface aluminum-hydroxyl groups owing to the presence of impurities of the following type:

$$>\text{Al-OH} + \text{H-Al}< \;\rightarrow\; >\text{Al-O-Al}< + H_2 \qquad (3)$$

On the other hand, more recently, Xiao et al.[9] attributed this peculiar peak to some microstructural arrangement including the release of residual stresses and recombination of dislocations. They proposed this interpretation considering a fact that they did not observe this exothermic peak for the unmilled/undoped $NaAlH_4$. However, their interpretation seems to be at least debatable. As clearly shown in Figure 3(a) as received $NaAlH_4$ also exhibits very well developed exothermic peak. Also Fan et al.[13] observed a clear exothermic peak for $NaAlH_4$ synthesized by ball milling for 48 h from NaH and Al components. It seems that the lack of the first exothermic peak in the experiments done by Xiao et al.[9] may have resulted from a relatively low heating rate of 4 °C/min which they used. Usually, the lower the heating rate in a DSC test, the worse the resolution of peaks to the extent that some naturally weak peaks can completely disappear. However, in the present work we clearly observed this exo peak at all three DSC heating rates of 5, 10 and 15 °C/min. Another factor may be a different type of DSC machine used by Xiao et al.[9] (STD Q600) than the one use in the present work and in the work of Fan et al.[13] (Netzsch).

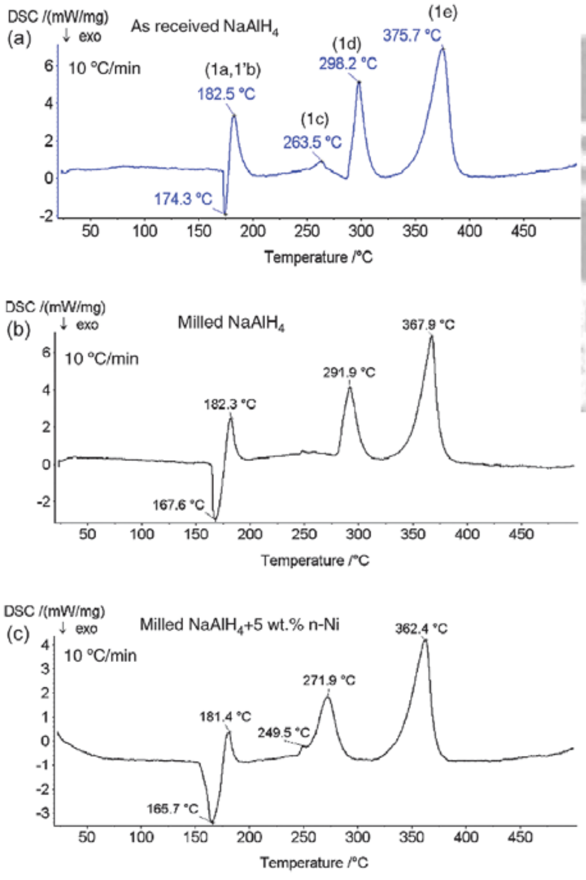

Fig. 3. DSC curves for (a) as received $NaAlH_4$, (b) ball milled $NaAlH_4$ and (c) ball milled $NaAlH_4$ + 5 wt% n-Ni. Heating rate 10 °C/min; high purity argon flow rate of 100 ml/min.

The first endothermic peak at 182.5, 182.3 and 181.4 °C in Figures 3(a), (b) and (c), respectively, can be attributed to a simultaneous melting and decomposition of $NaAlH_4$ into Na_3AlH_6, Al and H_2 according to reactions (1a, 1'b). The second weak endothermic peak at around 263.5–250 °C in Figures 3(a)–(c) is most likely attributed to the allotropic transformation of Na_3AlH_6 according to reaction (1c). The third strong endo peak at 298.2, 291.9 and 271.9 °C in Figures 3(a), (b) and (c), respectively, is attributed to the decomposition of Na_3AlH_6 into NaH, Al and H_2 according to reaction (1d). The interpretation of the reactions attributed to these two endothermic peaks conforms to the results reported by other researchers.[3,9,13,25,26] The third high temperature endo peak at 375.7, 367.9 and 362.4 °C in Figures 3(a), (b) and (c), respectively, is most likely attributed to the decomposition of NaH into Na (liquid) and H_2 (reaction (1e)). NaH is reported as decomposing at 425 °C.[27] The temperatures of the third high temperature endo peak in Figure 3 are approximately 50–60 °C lower than the quoted decomposition temperature of NaH. Dilts and Ashby[25] attributed this peak to the decomposition of NaH. Zaluski et al.[26] argued that the decomposition temperature of NaH may be significantly changed when NaH has been formed as a result of the decomposition of complex alanate like $NaAlH_4$. Therefore, with a high likelihood we can attribute the third high temperature endo peak in Figure 3 to the decomposition of NaH.

Comparing the peak positions in Figure 3 it is seen that ball milling alone seems to shift the temperatures of the first exothermic peak and reactions (1d) and (1e) to a slightly lower temperature range. The temperature of peak corresponding to the melting and decomposition of $NaAlH_4$ (reaction (1a, 1'b)) seems not to be affected by milling. A doping with 5 wt% n-Ni additionally shifts to a lower temperature range the peak corresponding to reaction (1d) by about 20 °C and (1e) by about 5 °C. However, in perspective, these temperature shifts are not substantial. A similar observation although with smaller temperature shifts was reported by Xiao et al.[9] for doping with Ti + Zr.

Figure 4 shows the Kissinger plots[1] for the determination of the apparent activation energy of reaction (1d) (decomposition of Na_3AlH_6) and (1e) (decomposition of NaH) during DSC tests at the heating rates of 5, 10 and 15 °C/min (DSC curves not shown here). It is to be mentioned that we were unable to determine the activation energy of reaction (1a, 1'b) because, for reasons which we do not clearly understand, at the highest heating rate of 15 °C/min the peak corresponding to reaction (1a, 1'b) (melting and decomposition of $NaAlH_4$) disappeared from the DSC curve for the ball milled $NaAlH_4 + 5$ wt% n-Ni nanocomposite as can be observed in Figure 5. Only the first exothermic peak at 169 °C, the small α to β-Na_3AlH_6 transformation peak and two endothermic peaks at 275.6 and 366.8 °C, attributed to reaction (1d) and (1e), respectively, are observed on a DSC curve. A similar disappearance of the melting peak accompanied by merging of the first decomposition peak of $LiAlH_4$ with the exothermic hydroxyl reaction peak (reaction (3)) was reported for the system $LiAlH_4 + 5$ wt% n-Ni.[16, 17] However, for $LiAlH_4 +$ 5 wt% n-Ni that phenomenon was observed to occur at heating rates of 5, 10 and 15 °C/min. It is possible that the elimination of melting of the $NaAlH_4 + 5$ wt% n-Ni nanocomposite is also caused by the n-Ni catalytic additive but it clearly appears only at the highest heating rate of 15 °C/min. Apparently, more research efforts are needed to understand this particular problem more clearly.

It can be seen in Figure 4(a) that for ball milled $NaAlH_4$ the apparent activation energy of the decomposition of Na_3AlH_6 (1d) is equal to ~140 kJ/mol. This value compares favorably to the value of ~121 kJ/mol reported by Sandrock et al.[28] for $NaAlH_4$ ball milled for 3 h as determined from the Arrhenius analysis of the isothermal desorption kinetics versus temperature. In Figure 4(b) the apparent activation energy of the decomposition of Na_3AlH_6 (reaction (1d)) is equal to ~101 kJ/mol for the milled $NaAlH_4 + 5$ wt% n-Ni. It is quite clear that the addition of nanometric Ni catalyst results in a substantial reduction of the apparent activation energy of the decomposition of Na_3AlH_6. The obtained here value of ~101 kJ/mol is comparable to the apparent activation energy of ball milled (3 h) $NaAlH_4$ doped with $TiCl_3$ catalytic precursors (0.9–6 mol.%) which was reported as being within the range of 97–98 kJ/mol.[28] Taking into account that the duration of ball milling in the present work was only 15 min vis-à-vis 3 h applied in Ref. [28] and different techniques were used in the present work (Kissinger) and in Ref. [28] (desorption curves) to determine the apparent activation energy, the agreement between the obtained values is quite remarkable. It can be concluded that the effect of nanometric Ni on the lowering of the apparent activation energy of the decomposition of Na_3AlH_6 has a very similar effect to metal chloride catalytic precursors such as $TiCl_3$ used in Ref. [28]

Figure 4(c) shows that the apparent activation energy of the decomposition of NaH (reaction (1e) in Fig. 3(a)) for the ball milled $NaAlH_4$ is equal to ~143 kJ/mol. This value is almost identical to the activation energy

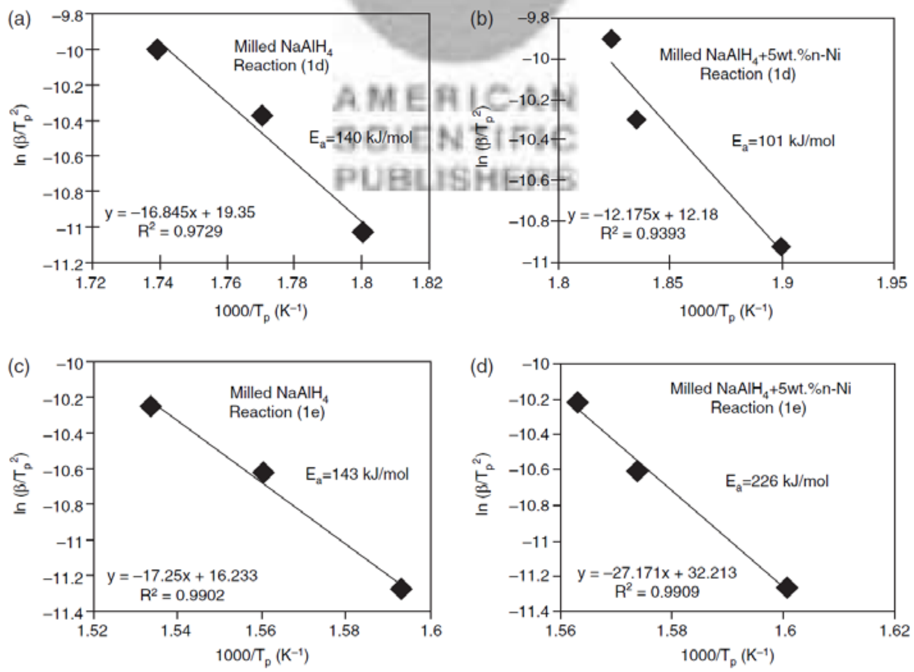

Fig. 4. The Kissinger plots for the determination of the apparent activation energy of dehydrogenation of ball milled $NaAlH_4$ and $NaAlH_4 + 5$ wt% n-Ni for (a, b) reaction (1e) [$1/3\beta$-Na_3AlH_6 (s)$\leftrightarrow$NaH (s)+1/3Al(s)+0.5H_2 (g)] and (c, d) reaction (1f) [NaH(s)$\rightarrow$Na (l)+0.5H_2].

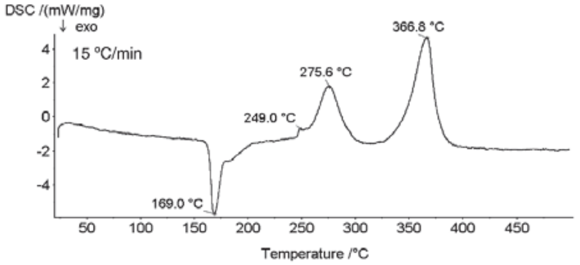

Fig. 5. DSC curve for $NaAlH_4 + 5$ wt% n-Ni at the heating rate of 15 °C/min; high purity argon flow rate of 100 ml/min.

value for the decomposition of Na_3AlH_6 as discussed above. However, the addition of 5 wt% n-Ni leads to an increase of the apparent activation energy to the value of ~226 kJ/mol as can be seen in Figure 4(d). Apparently, the catalytic nanometric Ni additive, which reduces the activation energy of the decomposition of Na_3AlH_6, acts in the opposite direction on the apparent activation energy of the decomposition of NaH which increases. Unfortunately, it is difficult to explain this peculiar behavior at the present moment. Also, we were unable to compare the values of the activation energy of the decomposition of NaH determined in this work to any values in the literature since they were impossible to be found. It seems that this is the first research work in which the apparent activation energy of the decomposition of NaH has been determined.

Figure 6 shows desorption curves registered at various temperatures for ball milled $NaAlH_4$ and $NaAlH_4 +$ 5 wt% n-Ni. Comparing Figures 6(a) and (b), showing desorption curves at 170 °C, it is quite obvious that the addition of n-Ni catalyst dramatically enhances the kinetics of hydrogen desorption for the ball milled $NaAlH_4 +$

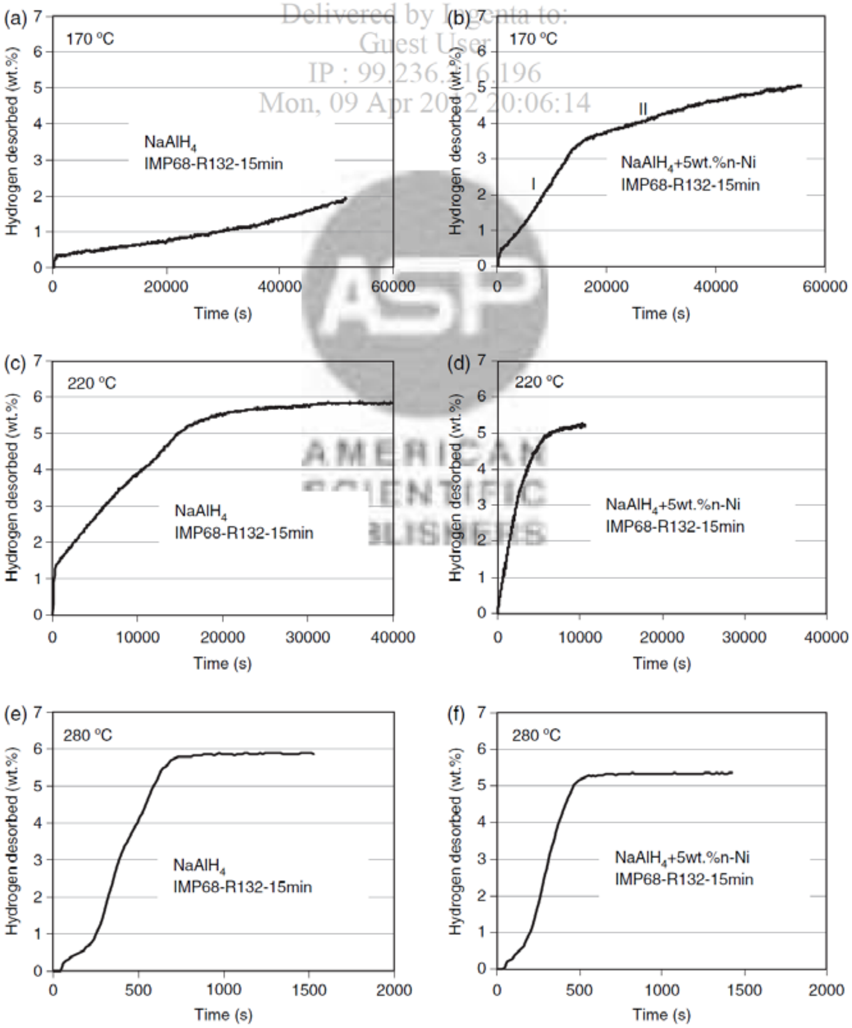

Fig. 6. Volumetric desorption curves under 0.1 MPa H_2 back pressure for ball milled undoped $NaAlH_4$ and $NaAlH_4 + 5$ wt% n-Ni at (a, b) 170 °C, (c, d) 220 °C and (e, f) 280 °C.

5 wt% n-Ni nanocomposite. The amount of hydrogen desorbed from ball milled undoped $NaAlH_4$ at 170 °C barely reaches 2 wt% after about 52,000 s (Fig. 6(a)). In contrast, the amount of hydrogen desorbed from the ball milled $NaAlH_4 + 5$ wt% n-Ni nanocomposite is 5 wt% after the same time duration (Fig. 6(b)). It is also seen that the desorption curve for the ball milled $NaAlH_4 +$ 5 wt% n-Ni nanocomposite in Figure 6(b) clearly exhibits two stages of desorption designated I and II. Stage I can be attributed to reaction (1”b) in which $NaAlH_4$ decomposes in a solid state because the desorption temperature (170 °C) is lower than the melting temperature of $NaAlH_4$ ($\sim$180 °C in Fig. 3(c)). Stage II is attributed to reaction (1d) in which β-Na_3AlH_6 decomposes in a solid state. During desorption at higher temperatures of 220 and 280 °C the amount of H_2 desorbed for ball milled undoped $NaAlH_4$ in Figures 6(c), (e) is slightly in excess of the purity-corrected hydrogen capacity for reactions (1”b) and (1d) which for a purity of 90% should be close to $\sim$5 wt%. It looks like either a supplier-specified purity is slightly higher than the one given in the specification or some quantities of non-H_2 impurities were released from the hydride. As discussed earlier, the presence of impurities in technical purity $NaAlH_4$ is, indeed, confirmed by XRD in Figure 2. The release of non-H_2 impurities in a first desorption for undoped $NaAlH_4$ was reported by Sandrock et al.[29] Interestingly, second and further desorptions did not released impurities anymore. For the first desorption for the $NaAlH_4 + 5$ wt% n-Ni nanocomposite at 220 and 280 °C in Figures 6(d) and (f), the amount of desorbed H_2 of about 5 wt% is much closer to the purity and n-Ni content corrected hydrogen capacity of about 4.8 wt% for reactions (1”b) and (1d). If this were the impurity release effect than it looks like n-Ni suppresses the decomposition of impurities.

It must be noted that we also carried out dehydrogenation of ball milled $NaAlH_4 + 5$ wt% n-Ni at 450 °C (desorption curve not shown here) and obtained 7 wt% H_2 desorbed after $\sim$500 s. Since the temperature of 450 °C is much beyond the third high temperature endothermic peak in Figure 3(a) the amount of desorbed H_2 confirms that reaction (1e) attributed to the decomposition of NaH must have been completed. In turn, this firmly confirms that the third high temperature endothermic peak in Figure 3 is indeed due to the decomposition of NaH.

The presence of hydride phases after desorption at various temperatures was investigated by XRD. Figure 7 shows XRD patterns after desorption at 170, 220 and 280 °C after desorption time corresponding to the end of each desorption curve in Figure 6 for ball milled undoped $NaAlH_4$ (Fig. 7(a)) and ball milled $NaAlH_4 + 5$ wt% n-Ni (Fig. 7(b)). It is clearly seen in Figure 7(a) that after desorption at 170 °C ($\sim$52,000 s; Fig. 6(a)) the microstructure still contains quite a substantial amount of retained $NaAlH_4$ and some amount of Na_3AlH_6 which agrees well with only $\sim$2 wt% H_2 desorbed in Figure 6(a). Apparently, for undoped ball milled $NaAlH_4$ this temperature is too low for a completion of reaction (1”b). What is interesting is the presence of two polymorphic forms of Na_3AlH_6 on the XRD pattern, one cubic (JCPDS 42-0786) and the other one non-cubic (JCPDS 20-1072). As mentioned earlier Claudy et al.[1, 3] reported that this polymorphic transformation occurred at about 252 °C (reaction (1c)). However, our results clearly show that the polymorphic transformation of Na_3AlH_6 can also occur isothermally at the temperature of 170 °C after relatively long dehydrogenation time. After desorption at 220 °C ($\sim$40,000 s; Fig. 6(c)) and 280 °C ($\sim$1,500 s; Fig. 6(e)) the XRD patterns in Figure 7(a) do not show the presence of diffraction peaks of both the $NaAlH_4$ and Na_3AlH_6. Only peaks of NaH and Al are present. It means that reactions (1”b) and (1d) are completed. Figure 7(b) shows that for $NaAlH_4 + 5$ wt% n-Ni after desorption at 170 °C ($\sim$56,000 s; Fig. 6(b)) the microstructure consists of both cubic and non-cubic polymorphs of Na_3AlH_6, NaH, Al and obviously the Ni additive. This result is in excellent accord with desorption of $\sim$5.2 wt% H_2 in Figure 6(b) indicating that reaction (1”b) was completed and reaction (1d) was still in progress. Obviously after dehydrogenation at 220 °C ($\sim$10,600 s; Fig. 6(d)) and 280 °C ($\sim$1,400 s; Fig. 6(f)) the microstructure consists of only NaH, Al and Ni indicating the completion of both reactions (1”b) and (1d). In conclusion, there is an excellent agreement with investigations by XRD in Figure 7 and volumetric desorption results in Figure 6. An increase of desorption temperature to 220 and especially to 280 °C in Figure 6 reduces the enhancement of the rate of desorption observed at 170 °C in Figure 6(b) for ball milled $NaAlH_4 + 5$ wt% n-Ni. Figures 6(c) and (d) show that at 220 °C the amount of 5 wt% H_2 is reached after $\sim$15,000 s for ball milled $NaAlH_4$ and after $\sim$7,000 s for ball milled $NaAlH_4 +$ 5 wt% n-Ni, respectively. Figures 6(e) and (f) show that at 280 °C the amount 5 wt% H_2 is desorbed within $\sim$600 and $\sim$480 s from ball milled $NaAlH_4$ and $NaAlH_4 + 5$ wt% n-Ni, respectively.

Table I shows a comparison of experimentally observed quantity of hydrogen desorbed at 170 °C within 18,000 s from ball milled $NaAlH_4 + 5$ wt% n-Ni in the present work with other catalytic precursors and metal catalysts used for $NaAlH_4$ desorbed at a similar temperature range. The desorption duration of 18,000 s was so chosen because desorption tests in some references were carried out only up to this time duration. In one case in Table I the desorption temperature is 125 °C which is much lower than the one in the present work to show a benefit of co-doping with two catalytic additives.[10] It is clearly seen from Table I that the n-Ni catalyst used in the present work compares very favorably with other additives used for the enhancement of dehydrogenation of $NaAlH_4$. The present n-Ni catalyst results in a faster desorption rate than carbon used in Ref. [30] and is

Table I. A comparison of the amount of hydrogen desorbed at 170 °C (under 1 bar H_2) from $NaAlH_4 + 5$ wt% n-Ni ball milled for 18,000 s in the present work with the data reported in the literature.

Dehydriding temperature (°C)	Dehydriding pressure (MPa)	Wt% H_2 desorbed after 18,000 s	Catalytic precursor/catalyst	Ball milling time (h)	Refs.	Comment
170	0.1	3.7	n-Ni	0.25	This work	Unpurified $NaAlH_4$
180	0.1	4.0	carbon	0.25	[30]	Unpurified $NaAlH_4$
165	0.1	4.2	micro-TiC	48	[13]	Synthesized $NaAlH_4$
150–165	0.13	6.0 (1)* 3.0 (3–5)#	Liquid Ti and Zr alkoxides	A few min.	[29]	Purified $NaAlH_4$
160	0.1	4.2	8% Ti+ 2% Zr	12	[9]	Synthesized $NaAlH_4$
150	?	3.0	$LaCl_3$	0.17	[11]	Unpurified $NaAlH_4$
125	0.1	4.0	$TiCl_4$+Zr	24	[10]	Unpurified $NaAlH_4$

Note: (1) *-after first cycle, possibly impurities; (3–5) #-after cycles 3–5; wt% normalized to the alanate only.

on par with micro-Ti[13] and liquid Ti and Zr alkoxides.[29] For the sake of clarity it should also be noted that the catalytic enhancement of dehydrogenation rate for the n-Ni doped $NaAlH_4$ observed in the present work is in disagreement with the results of Xueping et al.[11] who reported that the addition of 3 mol% of Ni to $NaAlH_4$ did not improve the desorption rate. Unfortunately, these authors did not report what kind of Ni they used in their experiments.

In general, slightly faster rates of desorption are observed for catalyzed $NaAlH_4$ which were synthesized by ball milling from NaH, Al and a catalytic additive involving a long milling time such as in Refs. [9, 13] or for commercial $NaAlH_4$+ catalyst mixtures milled for long time such as in Ref. [10] The best enhancement of desorption rate seems to occur by a co-doping of $NaAlH_4$ (unpurified) with $TiCl_4$ and elemental Zr which shows 4 wt% H_2 desorbed within 18,000 s at such a low temperature as 125 °C. However, one should note that this system was ball milled for a long time of 24 h. It must be pointed out that at least two experimental parameters such as the content of n-Ni and ball milling duration have not been optimized yet in the present work. We simply used in this work 5 wt% of the n-Ni dopant and 15 min milling time based on our results reported in Ref. [16] for n-Ni doped $LiAlH_4$. It is quite possible that the $NaAlH_4 + 5$ wt%n-Ni nanocomposite may need some further adjustment of these two parameters for better performance.

Whether or not the dehydrogenation rate enhancement after long milling duration is related to the powder particle size change is not obvious. On one hand Bogdanović et al.[4] reported faster dehydrogenation of Ti-doped ($Ti(OBu)_4$) $NaAlH_4$ having smaller particle size. On the other hand, Sandrock et al.[29] reported that ball milling even for longer times did not result in much particle size reduction. They observed a tendency to form agglomerated clusters of roughly 150 μm size. We also observed clustering of $NaAlH_4$ during ball milling.[1] Therefore, it seems that the refinement of a particle size of $NaAlH_4$ is not a principal factor responsible for faster desorption after long-term milling. It is quite possible that energetic ball milling is needed for creating a very homogeneous distribution of catalytic species within particles and on their surfaces, and their intimate contact with the $NaAlH_4$ matrix. According to a model put forward by Xiao et al.[9] for the case of metallic Ti and Zr catalysts there are two major mechanisms by means of which these catalytic dopants enhance the sorption properties of catalyzed $NaAlH_4$. The first one they called the "superficial catalytic process" where the active Ti-hydrides and Zr-hydrides formed during ball milling act as catalytic active sites on the surface of hydride matrix particles. Acting together they enhance synergistically the rate of decomposition of $NaAlH_4$. The second one they called the "favorable thermodynamic modification." The Ti and Zr dopants dissolve in the crystal lattice of $NaAlH_4$ forming $NaAl_{1-x}Ti_xH_4$ and $NaAl_{1-x}Zr_xH_4$ where Al^{3+} is partially substituted by Ti^{4+} and Zr^{4+}. Since the ionic radii of Ti^{4+} and Zr^{4+} are larger than that of Al^{3+} in the effect there is a lattice expansion which, in turn, leads to a more unstable hydride having a lower enthalpy change for its decomposition. Obviously, this model needs more experimental support especially using X-ray photoelectron spectroscopy (XPS) to be fully validated and accepted. Nevertheless, the above model is in accord with the experimental fact that a long ball milling duration seems to be beneficial for the enhancement of dehydrogenation rate as discussed earlier since it allows a very efficient process of homogeneous distribution of the catalytic active sites on the particle surfaces and within. However, it is not clear whether or not this model can be applied to the n-Ni catalyst in the present work. First, Ni does not form any hydride at ambient pressure so it can only act as a catalytic active site in a purely metallic form rather than in a hydride form. In addition, we recently reported for the $LiAlH_4 + 5$ wt% n-Ni nanocomposite[16, 17] that the melting of $LiAlH_4$ is eliminated only if the n-Ni particles are not only distributed on the surface of particles, as it occurs during simple mixing or low energy milling, but they are also embedded in the bulk of the particles for which a high energy ball milling is needed. With respect to the second mechanism, the "favorable thermodynamic modification" seems to be applicable for the n-Ni catalyst. The ionic radius of Ni^{2+} is 0.069 nm which is much larger than 0.051 nm for Al^{3+}.[31] Apparently, assuming a

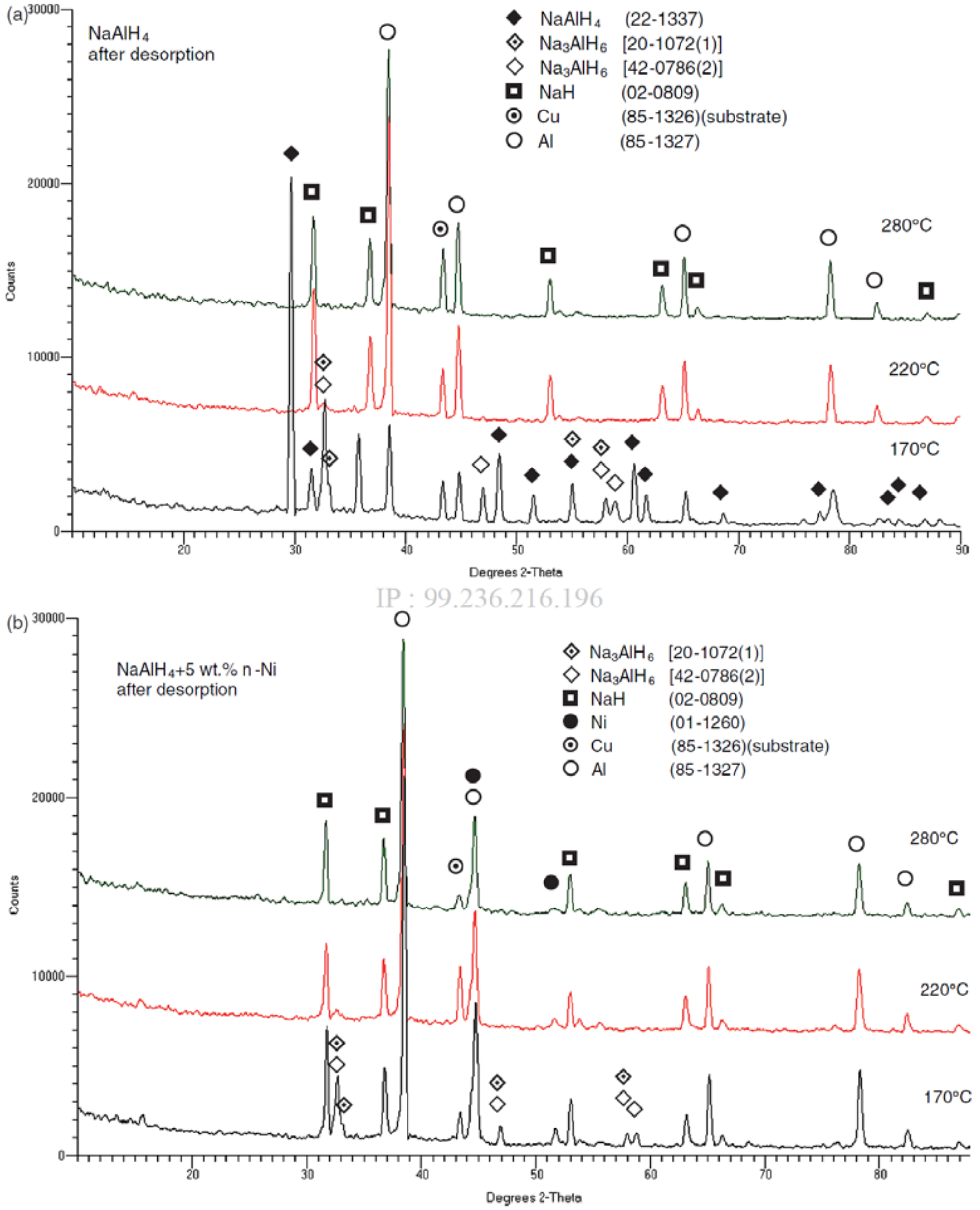

Fig. 7. XRD patterns after desorption at 170, 220 and 280 °C (after desorption time corresponding to the end of the desorption curve in Fig. 6). (a) Ball milled undoped $NaAlH_4$ and (b) ball milled $NaAlH_4 + 5$ wt% n-Ni.

partial solubility of Ni in $NaAlH_4$ by substituting Al, there should be a resulting lattice expansion. We have not carried out the lattice parameter studies in the present work which are required in future works together with the XPS studies. However, our most recent results[32] on adding catalytic nanometric Ni and Fe to $LiAlH_4$ show that the lattice expansion of $LiAlH_4$ increases with increasing ball milling energy, most likely, due to diffusion of Ni and Fe ions into $LiAlH_4$ during highly energetic ball milling. However, the model by Xiao et al.[9] ignores the electric charge difference between Al^{3+} and the catalytic ions like Ti^{4+}/Zr^{4+} and/or Ni^{2+}. This problem needs some more research.

4. CONCLUSIONS

The nanocomposites of $NaAlH_4$ doped with nanometric Ni (n-Ni) were processed by controlled ball milling for 15 min in a magneto-mill and subsequently investigated by Differential Scanning Calorimetry (DSC), X-ray diffraction

(XRD) and volumetric hydrogen desorption in a Sieverts-type apparatus. There is no reaction of n-Ni with the $NaAlH_4$ observed during milling. The apparent activation energies of the decomposition of Na_3AlH_6 and NaH in ball milled undoped and 5 wt% n-Ni doped $NaAlH_4$ were determined by the Kissinger method.[1] The value of the apparent activation energy of the decomposition of Na_3AlH_6 for ball milled undoped $NaAlH_4$ is ~140 kJ/mol as compared to its counterpart for ball milled $NaAlH_4 + 5$ wt% n-Ni which is equal to ~101 kJ/mol. The latter value is in a remarkable agreement with the apparent activation energy of 97–98 kJ/mol for ball milled (3 h) $NaAlH_4$ doped with $TiCl_3$ catalytic precursors (0.9–6 mol.%).[28] Therefore, it can be concluded that the effect of nanometric Ni on the lowering of the apparent activation energy of the decomposition of Na_3AlH_6 has a very similar effect to metal chloride catalytic precursors such as $TiCl_3$ used in Ref. [28] The apparent activation energy of the decomposition of NaH for the ball milled undoped $NaAlH_4$ is equal to ~143 kJ/mol. However, the addition of 5 wt% n-Ni leads to a substantial increase of the apparent activation energy of NaH to the value of ~226 kJ/mol. Apparently, the n-Ni additive somehow hinders the latter reaction.

Volumetric desorption tests indicate a substantial enhancement of the rate of hydrogen desorption at 170 °C for the ball milled $NaAlH_4 + 5$ wt% n-Ni composite as a result of the catalytic action of n-Ni. No reaction of n-Ni with the $NaAlH_4$ matrix is observed during dehydrogenation at 170–280 °C. The n-Ni catalyst used in the present work compares very favorably with other catalytic additives reported in the literature which were used for the enhancement of dehydrogenation of $NaAlH_4$.

Acknowledgments: This research was supported by the NSERC Hydrogen Canada (H2CAN) Strategic Research Network, NSERC Discovery and NSERC/Vale Inc. Collaborative Research and Development grants which are gratefully acknowledged. The authors would like to thank Dr. Vladimir Paserin and Mr. Steve Baksa of Vale Ltd. for producing and supplying the nanometric Ni powder used in this study. The authors are grateful to Prof. Linda Nazar from the Department of Chemistry, University of Waterloo, for the usage of XRD equipment.

References and Notes

1. R. A. Varin, T. Czujko, and Z. S. Wronski, Nanomaterials for Solid State Hydrogen Storage, Springer Science+Business Media, New York, NY **(2009)**, Chaps. 1 and 3.
2. B. Bogdanović and M. Schwickardi, *J. Alloys Compd.* 253, 1 **(1997)**.
3. P. Claudy, B. Bonnetot, G. Chahine, and J. M. Letoffe, *Thermochim. Acta* 38, 75 **(1980)**.
4. B. Bogdanović, R. A. Brand, A. Marjanović, M. Schwickardi, and J. Tölle, *J. Alloys Compd.* 302, 36 **(2000)**.
5. B. Bogdanović, U. Eberle, M. Felderhoff, and F. Schüth, *Scripta Materialia* 56, 813 **(2007)**.
6. K. J. Gross, G. Sandrock, and G. J. Thomas, *J. Alloys Compd.* 330, 691 **(2002)**.
7. B. Bogdanović, M. Felderhoff, A. Pommerin, F. Schüth, and N. Spielkamp, *Adv. Mater.* 18, 1198 **(2006)**.
8. J. Wang, A. D. Ebner, R. Zidan, and J. A. Ritter, *J. Alloys Compd.* 391, 245 **(2005)**.
9. X. Xiao, L. Chen, X. Wang, S. Li, C. Chen, and Q. Wang, *Int. J. Hydrogen Energy* 33, 64 **(2008)**.
10. T. Schmidt and L. Röntzsch, *J. Alloys Compd.* 496, 138 **(2010)**.
11. Z. Xueping, L. Shenglin, and L. Donglin, *Int. J. Hydrogen Energy* 34, 2701 **(2009)**.
12. B. Bogdanović, M. Felderhoff, S. Kaskel, A. Pommerin, K. Schlichte, and F. Schüth, *Adv. Mater.* 15, 1012 **(2003)**.
13. X. Fan, X. Xiao, J. Hou, Z. Zhang, Y. Liu, Z. Wu, C. Chen, Q. Wang, and L. Chen, *J. Mater. Sci.* 44, 4700 **(2009)**.
14. A. Zaluska, L. Zaluski, and J. O. Ström-Olsen, *J. Alloys Compd.* 298, 125 **(2000)**.
15. R. A. Varin, T. Czujko, and Z. S. Wronski, *Int. J. Hydrogen Energy* 34, 8603 **(2009)**.
16. R. A. Varin and L. Zbroniec, *J. Alloys Compd.* 506, 928 **(2010)**.
17. R. A. Varin, L. Zbroniec, T. Czujko, and Z. S. Wronski, *Int. J. Hydrogen Energy* 36, 1167 **(2011)**.
18. V. Paserin, S. Baksa, A. Zaitsev, J. Shu, F. Shojai, and W. Nowosiadly, *J. Nanosci. Nanotechnol.* 8, 4049 **(2008)**.
19. A. Calka and A. P. Radlinski, *Mater. Sci. Eng. A* 134. 1350 **(1991)**.
20. Patents: WO9104810, US5383615, CA2066740, EP0494899, AU643949.
21. A. Calka and R. A. Varin, Application of Controlled Ball Milling in Materials Processing, *International Symposium on Processing and Fabrication of Advanced Materials IX (PFAM IX)*, edited by T. S. Srivatsan, R. A. Varin, and M. Khor, ASM International, Materials Park, OH **(2001)**, pp. 263–287.
22. S.-I. Orimo, Y. Nakamori, J. R. Eliseo, A. Züttel, and C. R. Jensen, *Chem. Rev.* 107, 4111 **(2007)**.
23. H. P. Klug and L. Alexander, X-ray Diffraction Procedures for Polycrystalline and Amorphous Materials, John Wiley and Sons, New York **(1974)**, pp. 618–708.
24. J. Block and A. P. Gray, *Inorg. Chem.* 4, 304 **(1965)**.
25. J. A. Dilts and E. C. Ashby, *Inorg. Chem.* 11, 1230 **(1972)**.
26. L. Zaluski, A. Zaluska, and J. O. Ström-Olsen, *J. Alloys Compd.* 290, 71 **(1999)**.
27. CRC Handbook of Chemistry and Physics, 91st ed., 2010-2011, Section 4: Properties of the Elements and Inorganic Compounds (Interactive Table).
28. G. Sandrock, K. Gross, and G. Thomas, *J. Alloys Compd.* 339, 299 **(2002)**.
29. G. Sandrock, K. Gross, G. Thomas, C. Jensen, D. Meeker, and S. Takara, *J. Alloys Compd.* 330, 696 **(2002)**.
30. A. Zaluska, L. Zaluski, and J. O. Ström-Olsen, *J. Alloys Compd.* 298, 125 **(2000)**.
31. D. R. Askeland, P. P. Fulay, and W. J. Wright, The Science and Engineering of Materials, Cengage Learning, Stamford, CT **(2011)**, pp. 891–892.
32. R. A. Varin and R. Parviz, *Int. J. Hydrogen Energy* 10.1016/j.ijhydene.2012.02.182 (in press).

Received: 26 May 2011. Accepted: 14 June 2011.

6. PRACTICAL EXAMPLES OF IRREVERSIBLE HYDROGEN ENERGY STORAGE APPLICATIONS (MILITARY AND CIVILIAN)

Military applications

https://www.bloomberg.com/research/stocks/private/snapshot.asp?privcapId=28522405&goback=.cps_124714
9767187_1

Company Overview of Ardica Technologies, Inc.

Ardica Technologies, Inc. provides mobile power solutions for military and consumer markets worldwide. The company offers WFC20 System and Cartridge, a central power source system for dismounted soldiers to power their integrated soldier power/data systems and gears for missions ranging from several hours to several days; and fuel cell and chemical hydride fuel technology products. It offers batteries for mobile phones, smartphones, tablets, laptops, and other portable electronic devices. The company was founded in 2004 and is based in San Francisco, California.

Cartridge power on demand by Ardica

WFC20 System and Cartridge

They started with a unique chemical hydride fuel, and partnered with leading scientists and energy agencies to develop our proprietary composition, which we packaged into cartridges. Changing a cartridge takes just a few seconds and the WFC20 is ready to go again.

Details of the WFC20 System

The system is designed to enhance the performance of the Integrated Soldier Power/Data System (ISPDS) **vest**, commonly known as SWIPES. The combination of the Ardica WFC20 and the ISPDS will provide soldiers a new level of communication and network awareness for longer durations and less weight than competing technologies

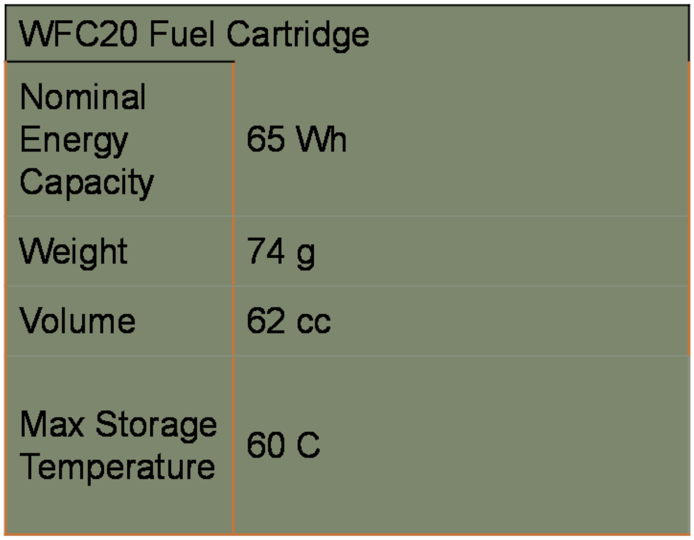

WFC20 Fuel Cartridge	
Nominal Energy Capacity	65 Wh
Weight	74 g
Volume	62 cc
Max Storage Temperature	60 C

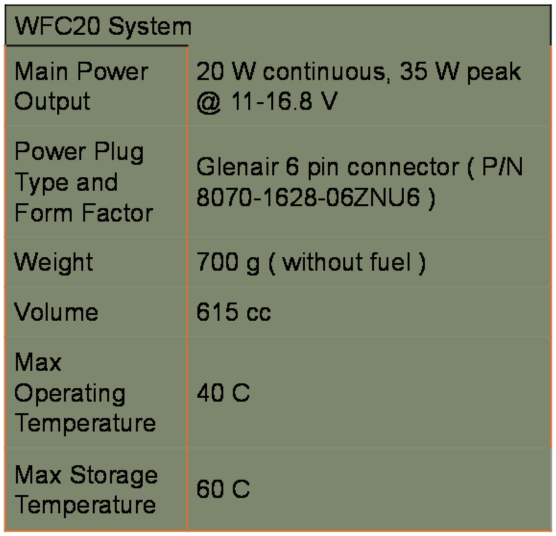

WFC20 System	
Main Power Output	20 W continuous, 35 W peak @ 11-16.8 V
Power Plug Type and Form Factor	Glenair 6 pin connector (P/N 8070-1628-06ZNU6)
Weight	700 g (without fuel)
Volume	615 cc
Max Operating Temperature	40 C
Max Storage Temperature	60 C

https://www.strategic-culture.org/news/2018/03/27/russia-game-changing-weapons-that-were-not-mentioned-in-putin-speech.html

Russia's Game-Changing Weapons That Were Not Mentioned in Putin's Speech

ARKADY SAVITSKY | 27.03.2018 | SECURITY / DEFENSE

This year, the Army-2018 exhibition will see **a light aircraft powered by a hydrogen-air engine (a fuel cell-my comment).** The forum is slated to be held August 21-26. **The concept behind this engine is known as "Electric Aircraft," which uses fuel cells as a power source to produce electrical energy without the combustion process.** The fuel used is hydrogen, which is transformed into electricity (? - my comment). **Such a plane could stay in the air for a very long time and would be very inexpensive. No other country has managed to make such an aircraft operational. It could be used for a multitude of various missions by the military and other security agencies.**

The West wanted to turn Russia into a backward country on its knees. This was a strategic mistake that instead encouraged it to stand tall and lead the way in the state-of-the-art technology race, forcing the US and its allies to lag behind.

http://www.expouav.com/news/latest/hydrogen-fuel-cells-drones/

June 5, 2017

Will Hydrogen Fuel Cells Help Drones Stay in the Air?

Juan Plaza

A few months ago we published an article about **the current limitations on time-in-the-air (TITA) for electric UAV's (Unmanned Aerial Vehicles)**. In that piece, we focused on **three alternatives to extend the amount of time that electric drones can remain in the air performing their mission. Tethered devices, solar power and in-the-field rapid battery replacements are the three viable** options that operators have today.

All three solutions presented considerable extensions to TITA, but have limitations associated with replacing conventional and commonly used technology with new, and in some cases, cumbersome alternatives. Now though, **the energy industry seems to be getting warmer (no pun intended) to the idea of Fuel Cell Power Systems (FCPS)** and the many advantages that this technology, **first proposed in 1838 by William Grove, bring to the table.**

Today, restrictions imposed on small commercially available (electric) drones of flying times of 25 minutes or less (depending on number of rotors and/or load) are being challenged by a number of manufacturers both here in the USA, Europe and China using fuel cells.

For the purpose of this article we focused on two innovators in the field of fuel cells: **Protonex, a wholly owned subsidiary of Ballard Power Systems (BLDP)** that is based in Massachusetts, and **MMC, headquartered in the province of Shenzhen, PR China. Both of these private companies are making significant inroads in the development and commercialization of FCPS for regular use in UAVs with missions which require longer time in the air.**

FCPS come in many forms. Some are more suitable for the world of light, small drones. Others are specifically designed and manufactured for large, industrial or military uses.

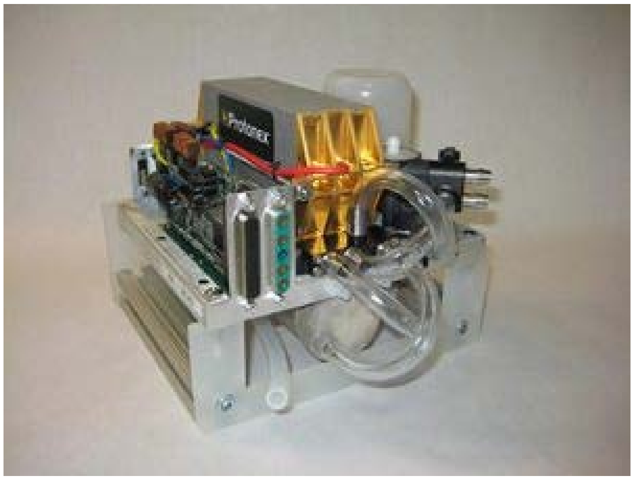

Protonex 550 Watt FC System

Protonex has focused on the use of Proton Exchange Membrane (PEM) technology for small, light UAV applications weighing less than 20 lbs. For this category they offer the SBH UAV Power System which is a PEM fuel cell operating at relatively low temperatures of 60° to 80° C (140°F to 175°F). This alternative offer quick start-up times, generating 350 W at full capacity. The hydrogen is stored in a chemical hydride cartridge and liberated as the system requires, while the oxygen comes from the air. The fuel cell is hybridized with a battery to provide peak power required for launch or climbing. The system features power generation 2 to 3 times the specific energy of LiPo batteries.

For **applications** that **require high payloads and are not heat sensitive Protonex offers PEM fuel cells running on compressed hydrogen with systems providing up to 1.4 kW of electricity.** When properly **integrated into a small fixed wing UAV**, **improvements over 5 times LiPo batteries have been demonstrated, including the 26 hour flight of the Ion Tiger**

by the Navy Research Laboratory (35 lbs including a 5 lbs payload). This technology is now making its way out of military systems and into commercial UAS.

Hydrogen Fuel Cell

Similarly, **MMC** has focused on the use of hydrogen as the main source of fuel for their power cells. **MMC is currently manufacturing and distributing two models of fuel cells, HyDrone 1800 & HyDrone 1550 with endurances (TITA) of 4.5 hours and 2.5 hours respectively.** When we inquired about the possibility of using these alternative power sources for commercially available UAVs other than the MMC drone models, **MMC officials clarified that their hydrogen fuel cells are designed for a wide range of popular commercial drones, both fixed-wing and multi-rotors, such as DJI M600, DJI M600 Pro and other heavy-payload drones.**

Hydrogen tank

The main advantage of fuel cells is the fact that they produce energy as required. That's different from batteries, which simply store energy and release it on demand. Every fuel cell requires two components. **One is the main body of the power-generating unit and the other is the fuel tank, being hydrogen or any other gas or liquid. However, since fuel cells use oxygen from the air for half the reaction, the energy density is much improved over batteries.**

According to MMC, **the fuel cell weight is in direct relationship to output power and the volume of fuel. In this case, hydrogen is directly proportionate to the requirements of flight.** In other words, **more fuel, more weight, hence more time in the air.** LiPo batteries can store and release electricity, while the fuel cell is mainly there to generate electricity, so the ratio between weight and power generation is fixed. **With fuel cells the tank size could be increased or decreased to fit a specific mission with the power generating unit staying the same.**

For example, **MMC's HPS-1800 hydrogen fuel cell can be compared in terms of weight vs. output power against a lithium battery. The weight of the HPS-1800 is 9.2kg, and its power output is 1800W, the potential energy storage in the hydrogen tank is 4500Wh, so its energy density is 490Wh/kg, which is twice that of the LiPo battery.**

When asked about the comparison between a fuel cell which requires an engine and a fuel tank, **strikingly similar to a small internal combustion engine, both manufacturers were adamant that the reliability of the fuel cells was considerably better.**

One key element of the advantage of fuel cells over internal combustion engines is the lack of moving parts and therefore complete absence of lubricants and a dramatic decrease in maintenance costs and unit replacement. While manufacturers of fuel cells are racing to lower weight and increase output, people on the battery side of the industry are skeptical fuel cells are the way of the future. **According to some engineers we interviewed for this article and who asked to remain anonymous, the current state of LiPo battery technology is plagued with inefficiencies.** Improvements to lithium batteries, which are possible with new materials, will make these batteries more efficient and comparable to fuel cells.

If we compare the energy density of today's LiPo to the equivalent product a decade ago we see a steady improvement of about 7% a year, which is definitely not a revolution, but a slow evolution.

Another big problem with **some fuel cells is that they generate a lot of heat,** approximately equivalent to the electricity produced up to 1,000ºC in some cases. Removal of the heat is an integration challenge in an industry where plastic is a large component of every small UAV. The use of delicate thermal or infrared sensors might be affected by this close source of temperature interference.

MMC Hydrogen Fuel Cell Copter

Fuel cells, especially low-temperature PEMs, are very effective and efficient for certain applications and **the extension of TITA is considerable. If the fuel cell manufacturers continue to mature this technology at the current rate, we could see a wave of small UAV products in the near future with a completely new set of capabilities. However, in order for these gains to be meaningful we need a regulatory environment that allows flights beyond visual line of sight (BVLOS).**

In the meantime though, the push to make this technology viable will continue, and the interest in seeing that happen will be coming from multiple places throughput the industry.

http://sputniknews.com/us/20160316/1036424754/lockheed-mach-6-hypersonic.html

Lockheed Closes in On Mach 6 Hypersonic Aircraft Technology

Lockheed Martin
US
23:14 16.03.2016 (updated 00:53 17.03.2016)

On Tuesday, defense giant Lockheed Martin announced it has made major technological breakthroughs that could lead to the development of a hypersonic aircraft capable of flying six times the speed of sound.

Last August, Airbus filed a patent for a passenger jet that travels at speeds of Mach 4.5, or 4.5 times the speed of sound. **Powered by onboard hydrogen**, the concept plane would use a **rocket engine to propel itself into the upper atmosphere before leveling off to a cruising speed of 3,000 miles per hour.**

Aerospace company Lockheed Martin is **developing an even faster military jet.** Speaking to reporters, Lockheed's chief executive Marillyn Hewson said that her company was on the verge of a major breakthrough.

"We are now producing a controllable, low-drag, aerodynamic configuration capable of stable operations from takeoff to subsonic, transonic, supersonic and hypersonic, to Mach 6," she claimed.

"We're proving a hypersonic aircraft can be produced at an **affordable price.** We estimate it will **cost less than $1 billion to develop, build, and fly a demonstrator aircraft the size of an F-22."**

The **key problem** facing hypersonic aircraft is making **a stable "scramjet" engine, which funnels oxygen from outside air to power the aircraft.** Lockheed claims to have found a solution, though Hewson didn't go into specifics.

Other breakthroughs include **new thermal protection systems**, key for defending **against friction at high speeds, as well as innovative aerodynamic shapes, navigation control improvements, and long-range communication capabilities.**

While the **first consideration for the Pentagon is military applications**, Hewson said that the **technology could ultimately apply to civilian use.**

"The technology could also enable hypersonic passenger flights, and, even easier, access to space," she said. "I am confident that Lockheed Martin has the technical expertise to make it happen."

The defense contractor plans to **develop its aircraft throughout the 2020s, with hypersonic planes ready to enter service in the 2030s.**

"We actually feel that we've made substantial progress in all the technologies associated with hypersonics," said Rob Weiss, executive vice president of Lockheed arm Skunkworks, according to Defense News.

"There's a number of challenges in the technologies, the propulsion, the materials that have to deal with the high temperatures, and we're at a point now where those technologies are mature, and therefore we feel very confident that we can field and successfully fly a hypersonic vehicle."

Still, **Lockheed may be far behind Chinese defense companies. Last November, Beijing conducted its sixth test flight of the DF-ZF, a hypersonic glide vehicle**.

"The **DF-ZF is an ultra-high-speed missile allegedly capable of penetrating US air defense systems based on interceptor missiles,"** Bill Gertz wrote for the Washington Free Beacon.

"**The DF-ZF was tracked by US intelligence agencies and flew at speeds beyond Mach 5,** or five times the speed of sound."